

Multi-Cluster, Mixed-Mode Computational Modeling of Human Head Conductivity

Adnan Salman¹, Sergei Turovets¹, Allen Malony¹ and Vasily Volkov²

¹ NeuroInformatics Center, 5219 University of Oregon, Eugene, OR 97403, USA
(adnan,sergei,malony)@cs.uoregon.edu

² Institute of Mathematics, Academy of Sciences, 11 Surganov St, Minsk 220072, Belarus
volk@im.bas-net.by

Abstract. A multi-cluster computational environment with mixed-mode (MPI + OpenMP) parallelism for estimation of unknown regional electrical conductivities of the human head, based on realistic geometry from segmented MRI up to 256^3 voxels resolution, is described. A finite difference multi-component alternating direction implicit (ADI) algorithm, parallelized using OpenMP, is used to solve the forward problem calculation describing the electrical field distribution throughout the head given known electrical sources. A simplex search in the multi-dimensional parameter space of tissue conductivities is conducted in parallel across a distributed system of heterogeneous computational resources. The theoretical and computational formulation of the problem is presented. Results from test studies based on the synthetic data are provided, comparing retrieved conductivities to known solutions from simulation. Performance statistics are also given showing both the scaling of the forward problem and the performance dynamics of the distributed search.

1 Introduction

The essence of most tomographic techniques is to determine unknown complex coefficients in PDEs governing the physics of the particular experimental modality. Such problems are typically non-linear and ill-posed. The first step in solving such an inverse problem is to find a numerical method to calculate the direct (*forward*) problem. When the physical model is three-dimensional and geometrically complex, the forward solution can be difficult to construct and compute. However, this is only the first stage of the tomographic solution. The second stage involves a search across a multi-dimensional parameter space of unknown (to be found) model properties. The search employs the forward problem with chosen parameter estimates and a function that determines the error of the forward calculation with an empirically measured result. As the error residuals of local inverse searches are minimized, the global search determines convergence to final property estimates based on its knowledge of how well the parameter space has been sampled.

Fundamental problems in neuroscience involving experimental modalities like electroencephalography (EEG) and magnetoencephalography (MEG) are naturally expressed as tomographic imaging problems. The difficult problems of *source localization* and *impedance imaging* require modeling and simulating the associated bioelectric fields.

Forward calculations are necessary in the computational formulation of these problems. Until recently, most practical research in this field has opted for analytical or semi-analytical models of a human head in the forward calculations [1, 2]. This is in contrast to approaches that use realistic 3D head geometry for purposes of significantly improving the accuracy of the forward and inverse solutions. To do so, however, requires that the geometric information be available from MRI or CT scans. With such image data, the tissues of the head can be better segmented and more accurately represented in the computational model. Unfortunately, these realistic modeling techniques have intrinsic computational complexities that grow as the image resolution increases. This is the primary reason such techniques have not been used in the past.

In source localization we are interested in finding the electrical source generators for the potentials that might be measured by EEG electrodes on the scalp surface. Here, the inverse search is looking for those sources (their position and amplitude) on the cortex surface whose forward solution most accurately describes the electrical potentials observed. The computational formulation of the source localization problem assumes the forward calculation is without error. However, this assumption in turn assumes the conductivity values of the modeled head tissues are known. In general, for any individual, they are not known. Thus, the impedance imaging problem is actually a predecessor problem to source localization. In impedance imaging, the inverse search finds those tissue impedance values whose forward solution best matches measured scalp potentials when experimental stimuli are applied. In either problem, source localization or impedance imaging, solving the inverse search usually involves the large number of runs of the forward problem. Therefore, computational methods for the forward problem, which are stable, fast and eligible for parallelization, as well as intelligent strategies and techniques for multi-parameter search, are of paramount importance.

To deal with complex geometries, PDE solvers use finite element (FE) or finite difference (FD) methods [3, 4]. The main computational idea behind these methods is to reduce a continuous problem with infinitely many unknown field values to a finite number of unknowns by discretizing the solution region into elements. Application of each of these approximation methods to the governing equations for the specific modality yields eventually a system of linear equations of the form $AX = b$, which must be solved to obtain the final solution. The solution techniques can be broadly categorized as direct and iterative solvers. The choice of the particular solution method is highly dependent upon the approximation technique employed to obtain the linear system, upon the size of the resulting system, and upon accessible computational resources.

Usually, for the geometry with the given complexity level, the FE methods are more economical in terms of the number of unknowns (the size of the stiffness matrix A , is smaller, as homogeneous segments do not need a dense mesh) and resulting computational cost. However, the FE mesh generation for a 3D, highly heterogeneous subject with irregular boundaries (e.g., the human brain) is a difficult task. The process involves a significant degree of preprocessing and smoothing of the initial geometry through manual means. A fully automated process of image segmentation and mesh generation is unavailable at present.

At the same time, the FD method with a regular cubed grid is generally the easiest method to code and implement. It is often chosen over FE methods for simplicity and

the fact that MRI/CT segmentation map is also based on a cubed lattice of nodes. Therefore, meshes are relatively easy to construct (once segmentation is accomplished) as the cubic/rectangular elements can be "mapped" directly from the voxels of the medical images (3D MRI scans). Many anatomical details (e.g., olfactory perforations and internal auditory meatus) or structural defects in case of trauma (e.g., skull cracks and punctures) can be included as the computational load is based on the number of elements and not on the specifics of tissues differentiation. Thus, the model geometry accuracy can be the same as the resolution of MRI scans (e.g., $1 \times 1 \times 1mm$), while in the FEM approach, simplification of the geometry is unavoidable as a result of mesh generation. In addition, the multiscale (multigrid) strategy of calculations on a hierarchy of coarser grids (starting with $64 \times 64 \times 44$ and feeding the results into the next cycle of iterations on the finer grid) can be easily implemented in a FD forward solver. The FD grid can be made non-uniform and/or applied in the spherical coordinates to capture more details in the regions of interest.

In the present work we adopt a model based on FD methods and construct a heterogeneous distributed and mixed-mode parallel simulation environment for conductivity optimization through inverse simplex search. FE simulation [7] is used to solve for relatively simple phantom geometries that we then apply as "gold standards" for validation.

2 Mathematical Description of the Problem

The relevant frequency spectrum in EEG and MEG is typically below $1kHz$, and most studies deal with frequencies between 0.1 and $100Hz$. Therefore, the physics of EEG/MEG can be well described by the quasi-static approximation of Maxwell's equations, the Poisson equation. The electrical *forward problem* can be stated as follows: given the positions, orientations and magnitudes of current sources, as well as geometry and electrical conductivity of the head volume Ω calculate the distribution of the electrical potential on the surface of the head (scalp) Γ_Ω . Mathematically, it means solving the linear Poisson equation:

$$\nabla \cdot \sigma(x, y, z) \nabla \phi(x, y, z) = S, \quad (1)$$

in Ω with no-flux Neumann boundary conditions on the scalp:

$$\sigma(\nabla \phi) \cdot n = 0, \quad (2)$$

on Γ_Ω . Here $\sigma = \sigma_{ij}(x, y, z)$ is an inhomogeneous tensor of the head tissues conductivity and S is the source current. Having computed potentials $\phi(x, y, z)$ and current densities $J = -\sigma(\nabla \phi)$, the magnetic field B can be found through the Biot-Savart law. In this paper, we do not consider anisotropy or capacitance effects (the latter because the frequencies of interest are too small), but they can be included in a straightforward manner. (Eq.(1) becomes complex-valued, and complex admittivity should be used.)

We have built a finite difference forward problem solver for Eq. (1) and (2) based on the multi-component alternating directions implicit (ADI) algorithm [8, 9]. It is a generalization of the classic ADI algorithm as described by Hielscher et al [6], but with improved stability in 3D (the multi-component FD ADI scheme is unconditionally

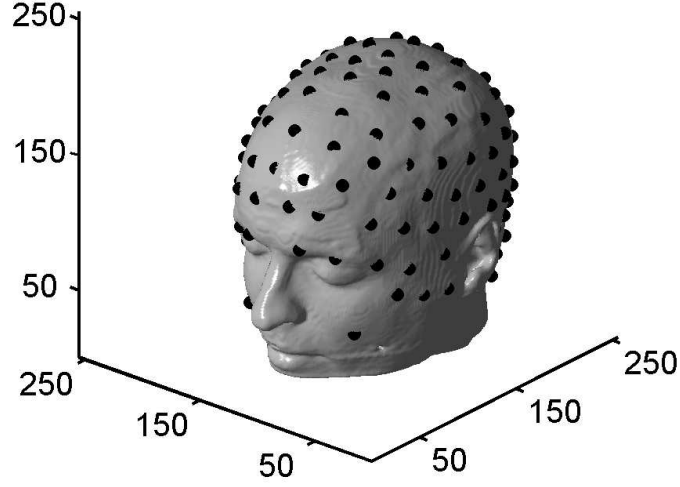


Fig. 1. A visualization of a 3D human head CT scan with the measuring electrodes

stable in 3D for any value of the time step [8, 9]). The algorithm has been extended to accommodate anisotropic tissues parameters and sources. To describe the electrical conductivity in the heterogeneous biological media within arbitrary geometry, the method of the embedded boundaries has been used. Here an object of interest is embedded into a cubic computational domain with extremely low conductivity values in the external complimentary regions. This effectively guarantees there are no current flows out of the physical area (the Neuman boundary conditions, Eq.(2), is naturally satisfied). The idea of the iterative ADI method is to find the solution of Eq. (1) and (2) as a steady state of the appropriate evolution problem. At every iteration step the spatial operator is split into the sum of three 1D operators, which are evaluated alternatively at each sub-step. For example, the difference equations in x direction is given as [9]

$$\frac{\phi_i^{n+1} - \frac{1}{3}(\phi_i^n + \phi_j^n + \phi_k^n)}{\tau} + \delta_x \phi_i^{n+1} + \delta_y \phi_j^n + \delta_z \phi_k^n = S, \quad (3)$$

where τ is a time step and $\delta_{x,y,z}$ is a notation for the appropriate 1D second order spatial difference operator (for the problems with variable coefficients it is approximated on a “staggered” mesh). Such a scheme is accurate to $O(\tau + \Delta x^2 + \Delta y^2 + \Delta z^2)$. In contrast with the classic ADI method, the multi-component ADI does not require the operators to be commutative. In addition, it uses the regularization (averaging) for evaluation of the variable at the previous instant of time.

It is worth noting, that the multi-component ADI algorithm can be also easily adapted for solving PDEs describing other tomographic modalities. In particular, we

have used it in other related studies, for example, in simulation of photon migration (diffusion) in a human head in near-infrared spectroscopy of brain injuries and hematomas.

The inverse problem for the electrical imaging modality has the general tomographic structure. From the assumed distribution of the head tissue conductivities, σ_{ij} , and the given injection current configuration, S , it is possible to predict the set of potential measurement values, ϕ^p , given a forward model F (Eq. (1), (2)), as the nonlinear functional [5, 6]:

$$\phi^p = F(\sigma_{ij}(x, y, z)). \quad (4)$$

Then an appropriate objective function is defined, which describes the difference between the measured, V , and predicted data, ϕ^p , and a search for the global minimum is undertaken using advanced nonlinear optimization algorithms. In this paper, we used the simple least square error norm:

$$E = \left(\frac{1}{N} \sum_{i=1}^N (\phi_i^p - V_i)^2 \right)^{1/2}, \quad (5)$$

where N is a total number of the measuring electrodes (cf. Fig. 1). To solve the nonlinear optimization problem in Eq.(5), we employed the downhill simplex method of Nelder and Mead as implemented by Press et al[3]. In the strictest sense, this means finding the conductivity at each node of the discrete mesh. In simplified models with the constraints imposed by the segmented MRI data, one needs to know only the average regional conductivities of a few tissues, for example, scalp, skull, cerebrospinal fluid (CSF) and brain, which significantly reduces the dimensionality of the parameter space in the inverse search, as well as the number of iterations in converging to a local minimum. To avoid the local minima, we used a statistical approach. The inverse procedure was repeated for hundreds sets of conductivity guesses from appropriate physiological intervals, and then the solutions closest to the global minimum solutions were selected using the simple criteria $E < E_{threshold}$.

3 Parallel Computational Design

The solution approach maps naturally to a multi-level computational design that can benefit from parallel execution both in the parametric search for conductivities and the forward problem calculations. Fig. 2 gives a schematic view of the approach we applied in a heterogeneous environment of parallel computing clusters. The *conductivity optimizer* (CO) is responsible for launching new inverse problems with guesses of conductivity values. Upon completion, the inverse solvers return conductivity solutions and error results to the master. Inverse solvers run on a separate computational server. The system design allows for the servers to be added dynamically and the number of processors per inverse solve to be decided at execution time, thus trading off inverse search parallelism versus forward problem speedup.

The CO interacts with each server using a TCP/IP-based interface. We use MPI to parallelize the inverse solvers as a master-worker computation. The *inverse master* (IM)

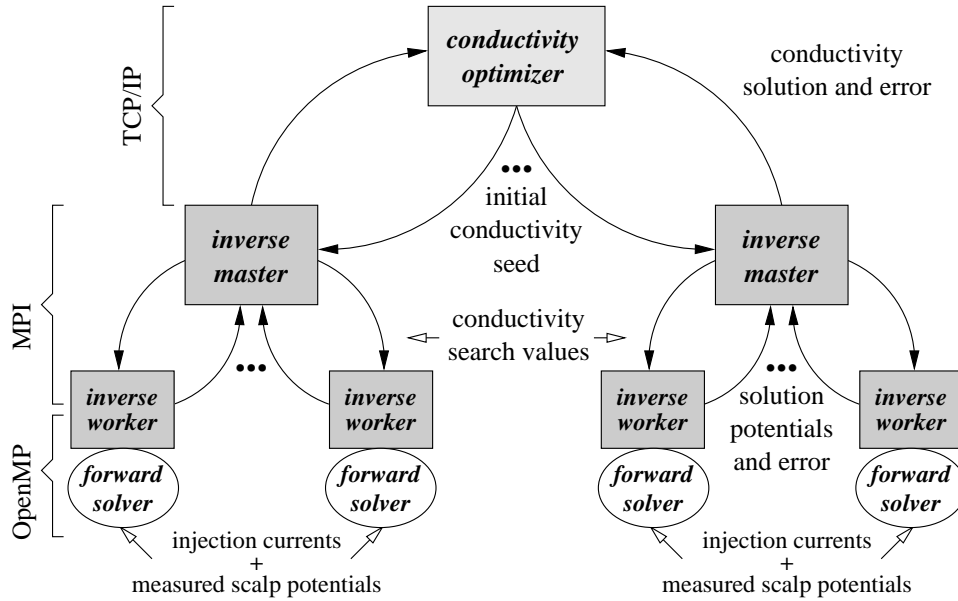


Fig. 2. Schematic view of the parallel computational system

manages multiple solvers at the same time. For each , the IM supplies new conductivity search values, lunches the simplex search and collects the results . The CO passes the initial seed to the IM to start simplex refinement for each new inverse worker. The IM sends a MPI message containing conductivity values to a free *inverse worker* (IW) to use in the forward calculation. The IM then waits to receives a solution from any IW, knowing which IW is working on what inverse solution. The *forward solver* (FS) is parallelized using OpenMP. It has been chosen over MPI as in the shared memory environment we avoid high data traffic naturally in solving PDE at 3D geometry. Parallelization of the ADI algorithm is straightforward, as it consists of nests of independent loops over “bars” of voxels for solving the effective 1D problem (Eq. (3)) at each iteration. These loops can be easily unrolled for efficient execution on a shared memory multiprocessor system.

The inverser solver MPI program executes as a mixed-mode parallel computation. Based on the number of cluster processors available and how the cluster is organized, we decide at runtime how many inverse workers to create and how many threads to assign to the forward calculation. In this manner, the program can be ported without change to both distributed memory and shared memory parallel clusters, and can naturally scale to meet available processing resources.

At the University of Oregon, we have access to a computational systems environment consisting of seven multiprocessor clusters. Of the shared memory clusters, three are 8-processor IBM Power4+ p655 machines, one is a 16-processor IBM Power4 p690 machine, and two (Phoenix and Optix) are 16-processor SGI Itanium-2 machines, an

Altix and Prism machine. The one distributed memory cluster is a Dell 16x2-processor Pentium Xeon machine. All of the clusters run Linux and are connected by a high-speed gigabit network. The conductivity optimizer can run on any machine, including a workstation. In our experiments below, we show results only for the shared memory clusters. Also, the mixed-mode inverse solve program allocated four threads for the OpenMP forward calculation in each inverse worker.

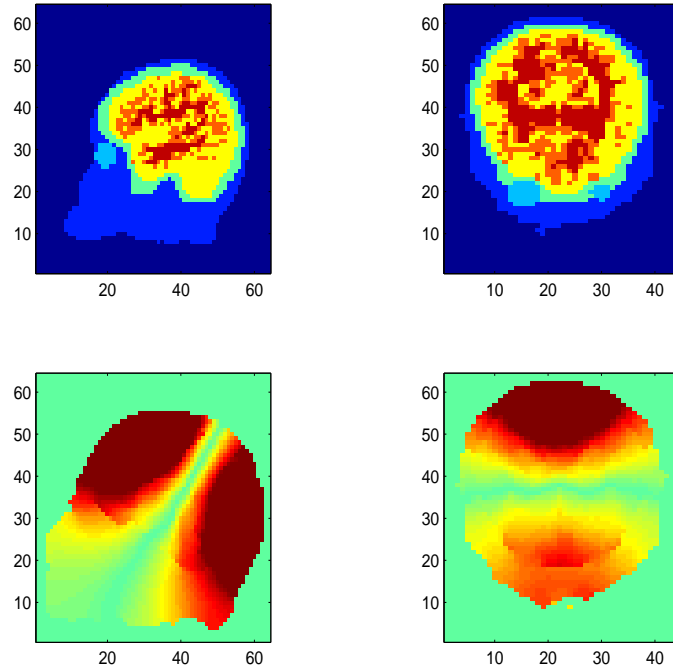


Fig. 3. Segmented MRI data ($64 \times 64 \times 44$ voxels resolution), top row, and calculated absolute value of potential, bottom row, for two points current injection (top and back of the head)

4 Computational Results

The forward solver was tested and validated against a 4-shell spherical phantom, and low ($64 \times 64 \times 44$) and high ($256 \times 256 \times 176$) voxels resolution human MRI data. For comparison purposes, the initial MRI data segmentation into ten tissues types as it is shown in the top row of Fig.3 was reduced to only four tissue types. Their values were set to those in the spherical model (cf. Table 1). We computed potentials at standard locations for the 129 electrodes configuration montage on the spherical phantom and compared the results with the analytical solution [2] available for a 4-shell spherical phantom in Fig. 4. One can see very good agreement, save for some minor discrepancies caused by the mesh orientation effects (the cubic versus spherical symmetry).

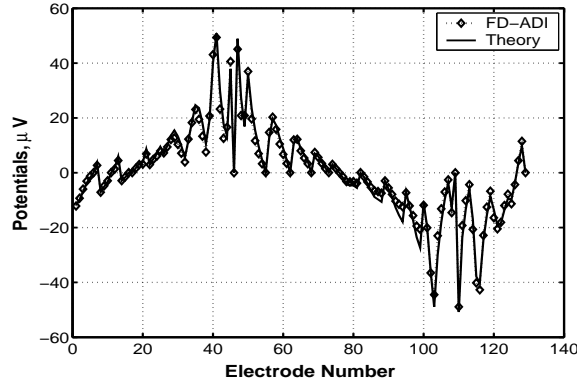


Fig. 4. Validation of the forward solver accuracy against analytics for a 4-shell spherical phantom.

Table 1. Tissues parameters in 4-shell models[2]

Tissue type	$\sigma(\Omega^{-1}m^{-1})$	Radius(cm)	Reference
Brain	0.25	8.0	Geddes(1967)
Csf	1.79	8.2	Daumann(1997)
Skull	0.018	8.7	Law(1993)
Scalp	0.44	9.2	Burger(1943)

Similarly, we found the good agreement for spherical phantoms between our results and the solution of the Poisson equation using the standard FEM packages such as FEMLAB [7]. Also, we have performed a series of computations for electric potentials and currents inside a human head with surgical or traumatic openings in the skull. We found that generally low resolution ($64 \times 64 \times 44$ voxels) like the one which is shown in the bottom row of Fig. 3 is not enough for accurate description of the current and potentials distribution through the head, as the coarse discretization creates artificial shunts for currents (mainly in the skull). With increased resolution ($128 \times 128 \times 88$ or $256 \times 256 \times 176$ voxels) our model has been shown to be capable to capture the fine details of current/potential redistribution caused by the structural perturbation. However, the computational requirements of the forward calculation increase significantly.

The forward solver was parallelized using OpenMP. The performance speedups (execution times) for $256 \times 256 \times 176$ sized problems on the IBM and SGI machines are shown in Fig. 5. While the performance is reasonable at present, we believe there are still optimizations that can be made, particularly on the SGI machines. The importance of understanding the speedup performance on the cluster compute servers is to allow flexible allocation of resources between inverse and forward processing.

To investigate the best balance of parallelism between inverse and forward processing, we conducted an experiment to optimize the numbers of MPI tasks and openMP threads at 12 processors of the 16-processors p690 machine. In this experiment we considered the total number of forward solutions performed by the cluster for several

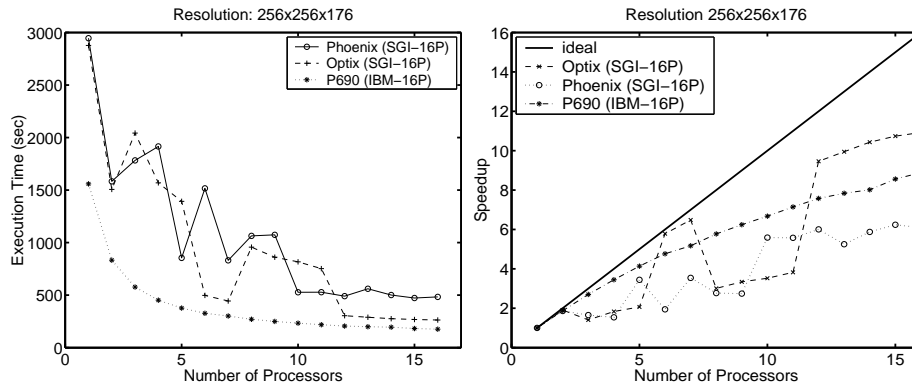


Fig. 5. Execution time (left) and speed-up (right) of the forward solver for grid size 256^3 on SGI (Phoenix, Optix) and IBM (p690) machines.

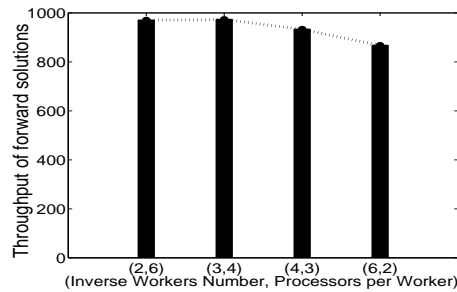


Fig. 6. Forward solutions throughput for different resource allocations between the forward and inverse problems. The total number of available processors is fixed to 12 in all configurations.

configurations in a fixed period of time. The number of iterations per a forward solution was fixed. The total number of forward solutions performed by a given cluster configuration was chosen as the figure of merit over the number of total inverse solutions due to the variation of the required number of forward computations in different inverse searches. The results are presented at Fig. 6. It can be seen that allocation of four threads per an inverse worker (3x4) gives the highest throughput for the total number of forward solutions.

In the inverse search the initial simplex was constructed randomly based upon the mean conductivity values (cl. Table 1) and their standard deviations as it is reported in the related biomedical literature. In the present test study we did not use the real experimental human data, instead, we simulated the experimental set of the reference potentials V in Eq. 5 using our forward solver with the mean conductivity values from Table 1, which had been assumed to be true, but not known a priori for a user running the inverse procedure. The search was stopped when one or two criteria were met. The first is when the decrease in the error function is fractionally smaller than some toler-

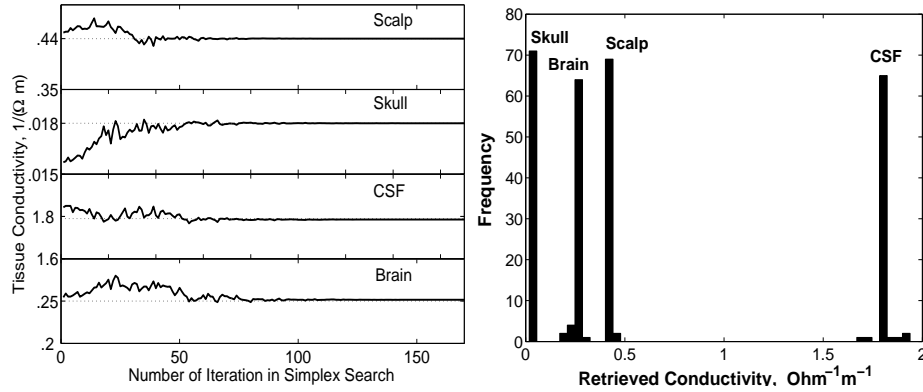


Fig. 7. Results of the inverse search. Dynamics of the individual search (left) and statistics of the retrieved conductivities for about 200 initial random guesses. The actual number of the solutions shown is 71, their error function is less than 1 microvolt.

ance parameter. The second is when the number of steps of the simplex exceeds some maximum value. During the search, the conductivities were constrained to stay within their pre-defined plausible ranges. If the simplex algorithm attempted to step outside of the acceptable range, then the offending conductivity was reset to the nearest allowed value. Our procedure had the desired effect of guiding the search based on prior knowledge. Some number of solution sets included conductivities that were separated from the bulk of the distribution. These were rejected as outliers, based on the significant larger square error norm in Eq. (5) (i.e., the solution sets were filtered according to the criteria $E < E_{threshold}$). We have found empirically that setting $E_{threshold} = 1\mu V$ in most of our runs produced a fair percentage of solutions close to the global minimum.

The distribution of the retrieved conductivities is shown in Fig. 7 (right). The fact that the retrieved conductivities for the intracranial tissues (CSF and brain) have wider distributions is consistent with the intuitive physical explanation that the skull, as having the lowest conductivity, shields the currents injected by the scalp electrodes from the deep penetration into the head. Thus, the deep intracranial tissues are interrogated less in comparison with the skull and scalp. The dynamics of an individual inverse search convergence for a random initial guesses is shown in Fig. 7 (left). In general, the conductivities for the extra cranial tissue and skull converge somewhat faster than the brain tissues, due to the better interrogation by the injected current.

After filtering data according to the error norm magnitude, we fitted the individual conductivities to the normal distribution. The mean retrieved conductivities $\sigma(\Omega^{-1}m^{-1})$ and their standard deviations $\Delta\sigma$ are: Brain (0.24 / .01), CSF (1.79 / .03), Skull (0.0180 / .0002), and Scalp (0.4400 / .0002). It is interesting to compare these values to the "true" conductivities from Table 1. We can see excellent estimates for the scalp and skull conductivities and a little bit less accurate estimates for the intracranial tissues. We also have done some preliminary runs with the realistic noise included. These runs and the similar investigation in Ref. [2] for a spherical phantom suggest that noise leads

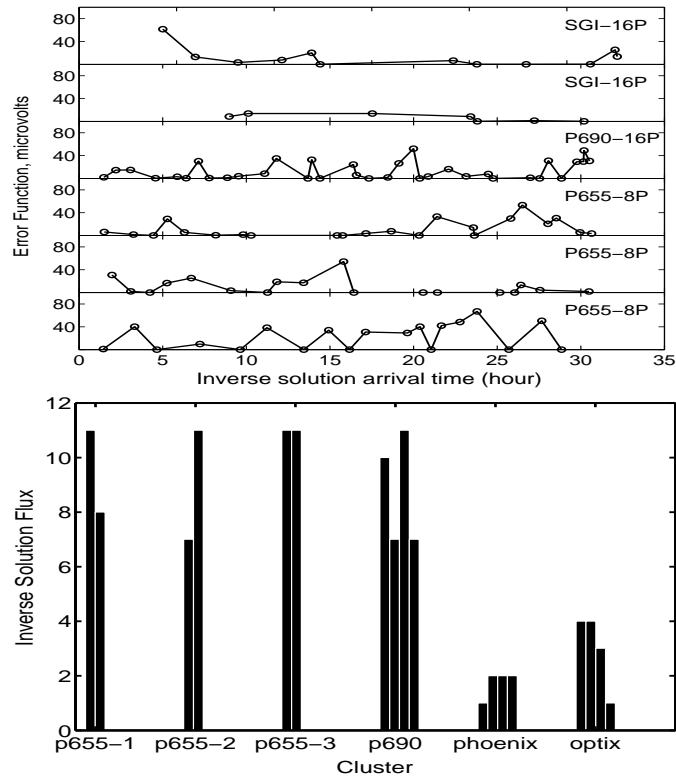


Fig. 8. Solutions flow at the conductivity optimizer (top). Inverse solutions arrival to the conductivity optimizer is marked. Number of inverse solutions per inverse worker (bottom).

to some deterioration of the distributions and more uncertainty in the results. In general, it still allows the retrieval of the unknown tissue parameters.

Finally, in Fig. 8 we present the dynamics of the performance of the inverse search in our distributed multi-cluster computational environment. Six curves with different markers show the dynamics of the inverse solution flux at the conductivity optimizer. The markers correspond to the instances of inverse solutions arrival to CO from a specific inverse master (cluster). The inverse solution rate varies between the clusters based on several factors: the number of processors available, the speed of the forward solve, and inverse search convergence rate. The markers seated at the "zero" error function line represent solutions that contribute to the final solution distribution, with the rest of the solutions rejected as outliers. In average, the throughput was 15 minutes per one inverse solution for the $128 \times 128 \times 88$ MRI resolution test case. The second graph shows the number of inverse solutions completed by the different clusters. Since we chose four threads to use in the OpenMP forward solve, the graph shows the number of inverse solutions completed per inverse worker.

5 Conclusion

We have built an accurate and robust 3D Poisson solver based on a finite difference multi-components ADI algorithm for modeling electrical and optical problems in heterogeneous biological tissues. We focus in particular on modeling the conductivity properties of the human head. The computational formulation utilizes realistic head geometry obtained from segmented MRI datasets. This is important to the effective use of impedance imaging and source localization in clinical neuroimaging applications where diagnostic accuracy depends significantly on the degree to which individual differences in head structure can be represented. The computational formulation of the problem is as a multi-cluster mixed-mode calculation suitable for parallel execution on a computational grid. Our results validate FDM approach for impedance imaging and provide a performance assessment of parallel computation on six clusters of the University of Oregon's ICONIC grid

In the future, we will enhance the computational framework in several ways. Additional cluster resources will be used to naturally scale the performance of the conductivity optimization. In particular, we will add the 16-node, 2-processor per node Dell cluster to the mix. Consistent with the ICONIC grid, our intent is to evolve the present interprocess communication (IPC) socket-based code to one that uses grid middleware support, allowing the impedance imaging program to more easily access available resources and integrate with neuroimaging workflows. Finally, intrinsically parallel multi-component ADI algorithms [9] in a forward solver and more intelligent schemes of conductivity search based on multi-resolution approaches could be tried. The idea here is to first start with fast, low-resolution solutions which can then narrow the range of and guide initial conductivity guesses for high-resolution, more accurate investigation.

References

1. Gulrajani, R.M.: Bioelectricity and Biomagnetism. John Wiley & Sons, New York (1998)
2. Ferree, T. C., Eriksen, K. J., Tucker, D. M.: Regional head tissue conductivity estimation for improved EEG analysis. *IEEE Transactions on Biomedical Engineering* 47(2000) 1584-1592
3. Press, W.H., Teukolsky, S.A., Vetterling, W.T., Flannery, B.P.: *The Numerical Recipes in C: The art of Scientific Computing*. 2nd edition. Cambridge University Press, New York (1992)
4. Jin, J.: *The Finite Element Method in Electromagnetics*. John Wiley & Sons, New York(1993)
5. Arridge, S.R.: Optical tomography in medical imaging. *Inverse Problems*, 15 (1999) R41-R93
6. Hielscher, A.H., Klose, A.D., Hanson, K.M.: Gradient Based Iterative Image Reconstruction Scheme for Time-Resolved Optical Tomography. *IEEE Transactions on Medical Imaging*. 18 (1999) 262-271.
7. <http://www.comsol.com>
8. Abrashin, V.N., Dzuba, I.A.: Economical Iterative Methods for solving multi- dimensional problems in Mathematical Physics. *Differential Equations* 30 (1994) 281-291
9. Abrashin, V.N., Egorov, A.A., Zhadaeva, N.G.: On the Convergence Rate of Additive Iterative Methods. *Differential Equations*. 37 (2001) 867-879